analytical chemistry

Open Access

pubs.acs.org/ac

Technical Note

Electrochemical Methods in the Cloud: FreiStat, an IoT-Enabled Embedded Potentiostat

David Bill,[#] Mark Jasper,[#] Andreas Weltin, Gerald A. Urban, Stefan J. Rupitsch, and Jochen Kieninger*

Cite This: *Anal. Chem.* 2023, 95, 13003−13009

Read Online

ACCESS | Metrics & More | Article Recommendations | Supporting Information

ABSTRACT: Embedded potentiostats enable electrochemical measurements in the Internet-of-Things (IoT) or other decentralized applications, such as remote environmental monitoring, electrochemical energy systems, and biomedical point-of-care applications. We report on Freiburg's Potentiostat (FreiStat) based on the AD5941 potentiostat circuit from Analog Devices, together with custom firmware, as the key to precise and advanced electrochemical methods. We demonstrated its analytical performance by various cyclic voltammetry measurements, advanced techniques such as differential pulse voltammetry, and a lactate biosensor measurement with currents in the nA range and a resolution of 54 pA. The FreiStat yielded analytical results comparable to benchtop devices and outperformed current commercial embedded potentiostats at significantly lower cost, smaller size, and lower power consumption. Decentralized corrosion analysis by a Tafel plot using the IBM Cloud showed its applicability in a typical IoT scenario. The developed open-source software framework facilitates the integration of electrochemical instrumentation into applications utilizing machine learning and other artificial intelligence. Together with the affordable and highly capable embedded potentiostat, our approach can leverage analytical chemistry toward increasingly important, more widespread and decentralized applications.

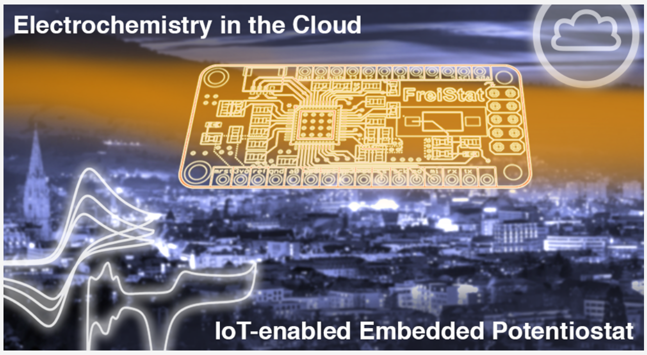

Electrochemical sensors and biosensors are the most diverse sensor family but, at the same time, are seen only a little in Internet-of-Things (IoT) scenarios. Numerous domains would benefit from sensor nodes in a cloud, ranging from environmental monitoring at remote places to systems for in situ corrosion analysis, chemical sensors part of electrochemical energy systems, and the biomedical field comprising point-of-care and ambient-assisted-living domains.[1,2] While the different application areas are strong drivers, a significant restriction is the availability of an embedded potentiostat with an appropriate software framework that enables numerous electrochemical methods and integrates various connection schemes or cloud services. Additionally, many applications require a small form factor and low power consumption, excluding well-established benchtop instrumentation devices.

Within the past decade, several embedded potentiostats, most of them with open-source software and open hardware, were developed, either based on operational amplifier circuits[3−13] or integrated circuits (ICs) with potentiostat functionality. The latter use the LMP91000 potentiostat IC from Texas Instruments,[14,15] the AD5940/AD5941 from Analog Devices,[16−19] or the ADuCM355 from Analog Devices, which comprises an analog front-end comparable to the AD5940/AD5941 but additionally an ARM Cortex-M3 processor. A particular case is the commercially developed EmStat Pico Module (PalmSens, The Netherlands), an OEM module based on the ADuCM355 with proprietary firmware and the possibility to communicate by the manufacturer's scripting language or to the software which also operates benchtop potentiostats.[20] Also, the Programmable System on a Chip (PSoC) from Cypress Semiconductor was used to implement a potentiostat.[21] A potentiostat dedicated to fast-scan cyclic voltammetry (FSCV), but with two electrodes only, is the TinyFSCV.[22]

Apart from serial interfacing to a computer, different wireless connections were used: NFC/RFID, Bluetooth, or Wi-Fi using the appropriate modules. The SIC4341 (Silicon Craft Technology PLC, Thailand) is an NFC tag integrated circuit comprising a potentiostat.[23] Some of the embedded potentiostats mentioned above demonstrated the usage of a cloud service, mainly for data storage.[8−10]

From an instrumentation point of view, the AD5940/AD5941 (or the ADuCM355 with comparable analog front-end) from Analog Devices will be the best choice when asking

Received: May 15, 2023
Accepted: August 4, 2023
Published: August 15, 2023

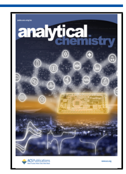

https://doi.org/10.1021/acs.analchem.3c02114
Anal. Chem. 2023, 95, 13003−13009

for a wide variety of electrochemical methods.[24] Still, the state-of-the-art of practically realized embedded potentiostats falls from an electrochemical perspective much behind benchtop devices. Especially in linear scan voltammetry or cyclic voltammetry, the discrepancy between the assumed ideal electric voltage ramp and the staircase from the digital signal generation in actual experiments plays a crucial role in the validity of the results. In some cases, features in a cyclic voltammogram are missing, or the charge that can be calculated from the curve is vastly underestimated. Apart from using an analog voltage ramp, specific data acquisition schemes for the electric current compensate for possible adverse effects. Integrating or averaging the current over each voltage step leads to results indistinguishable from a proper voltage ramp.[25] All of the above-described works on embedded potentiostat systems lack this capability of approaching the results from an ideal voltage ramp.

Therefore, we developed Freiburg's Potentiostat (FreiStat) relying on the AD5941 potentiostat circuit and brought it into the "Feather" format from Adafruit, providing access to a family of controller and accessory boards, allowing different applications with data storage on an SD card or connectivity through Wi-Fi, Ethernet, RFM69 radio, LoRa, Bluetooth, etc. The FreiStat provides typical features of an embedded potentiostat, like a small form factor (footprint less than 12 cm^2), low power consumption (below 100 mW without considering the power for Wi-Fi), or low budget (less than 80 €), but at the same time offers the analytical performance of benchtop devices with prices of several k€ or beyond. The open-source aspect allows for the understanding of the acquisition scheme in advanced methods, information that is often not accessible with commercial devices. We see FreiStat, apart from typical IoT or field applications, also in the domain of chemo- and bioanalysis when price or size plays a role, but analytical performance cannot be compromised.

■ SYSTEM DESIGN

Potentiostat Platform. The critical element of the FreiStat is the AD5941 from Analog Devices, which provides the necessary analog front-end (AFE) to perform amperometry, voltammetry, potentiometry, or electrochemical impedance spectroscopy (EIS, not yet implemented in the software framework) on a connected three-electrode electrochemical cell or sensor. The chip allows configuration through the Serial Peripheral Interface (SPI) via a microcontroller unit (MCU). Here, an Adafruit Feather M0 WiFi board is used, which features an Atmel SAMD21 controller and the ATWINC1500 module for cloud connectivity via Wi-Fi. The system allows power from a lithium-ion/lithium-ion polymer battery or USB cable. If needed, the FreiStat firmware could be easily ported to other MCUs. To connect the potentiostat chip to the MCU board, it is placed on a custom-designed printed circuit board that can be stacked on the Feather, a so-called "FeatherWing" (Figure 1). The PCB comprises the external passive elements for AD5941 and the electrochemical cell or sensor connector. Figures S1 and S2 in the Supporting Information provides the circuit diagram and board layout of the FreiStat main board.

The AD5941 features two analog loops interfacing with the electrochemical cell or sensor. The low-bandwidth loop consists of a dual-output digital-analog converter (DAC) with 6-bit and 12-bit output. A control amplifier (CA) and a low-power transimpedance amplifier (LPTIA) complete the potentiostat circuit. The low-bandwidth loop handles signals between DC and 200 Hz, matching most voltammetric methods. The high-bandwidth loop, designed for frequencies of up to 200 kHz, supports EIS measurements. The measurements in this work used the low-bandwidth loop, resulting in a configuration as shown in Figure 2.

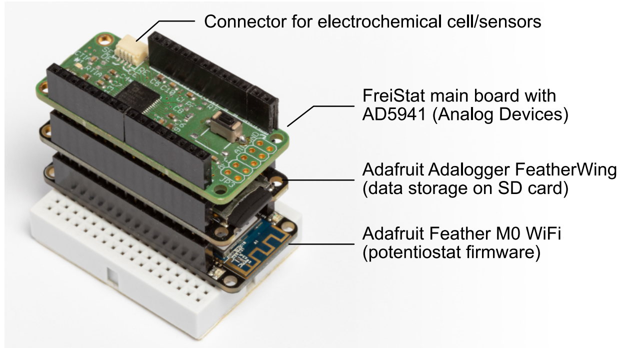

Figure 1. FreiStat with its core, the printed circuit board hosting the AD5941 in the format of a "FeatherWing".

The working electrode (WE) connects to the transimpedance amplifier (TIA), and the CA controls the counter electrode (CE). The applied cell potential of the WE with respect to the reference electrode (RE) is the difference between pin SE0 and pin RE0 by a combination of both DAC channels, which can both set voltages between 0.2 and 2.4 V with respect to the circuit's ground. The 12-bit DAC output applies the bias potential V_{BIAS} to the control amplifier, while the 6-bit DAC output defines the internal zero-level V_{ZERO} for the WE. The default configuration in the FreiStat firmware uses a fixed value for V_{ZERO}, while the V_{BIAS} is set according to the electrochemical method. This approach avoids a glitch while scanning over 0 V (further description and measurement in Supporting Information, Figure S3) and results in a practically usable potential range of ±2.0 V.

The feedback resistor of the TIA defines the current range. The programmable internal resistor R_{TIA} provides values between 1 and 512 kΩ, resulting in maximal currents of ±900 μA down to ±1.8 μA. Alternatively, the circuit allows switching an external resistor into the loop. The voltage output of the TIA passes via the ADC input multiplexer (MUX) through a programmable gain amplifier (PGA), an antialiasing filter (AAF) to the 16-bit ADC, providing a current resolution in the lowest current range of 54 pA (PGA set to gain 1). The external calibration resistor R_{CAL} allows calibration of the internal feedback resistor R_{TIA} of LPTIA to improve the accuracy of the current measurements. The FreiStat triggers the calibration each time a method is set up.

A postprocessing block (PPB) applies two digital low-pass filters reducing the data rate from the initial 800 kHz by a configurable factor (oversampling rate) and thus also the noise in the measurement signal. With a typical overall oversampling rate of, e.g., 1334, the data rate decreases to 600 Hz. Optionally a 50/60 Hz digital notch filter prevents the influence of the mains frequency.

The execution of the electrochemical methods and, thereby, the timing, relies on the sequencer of the AD5941. The sequencer is a hardware block capable of reading commands from the internal SRAM and performing timing commands or register writes to control the AFE and the measurement stage. From the MCU's firmware, different sequences can be preprogrammed into the SRAM (e.g., for setting potentials

https://doi.org/10.1021/acs.analchem.3c02114
Anal. Chem. 2023, 95, 13003−13009

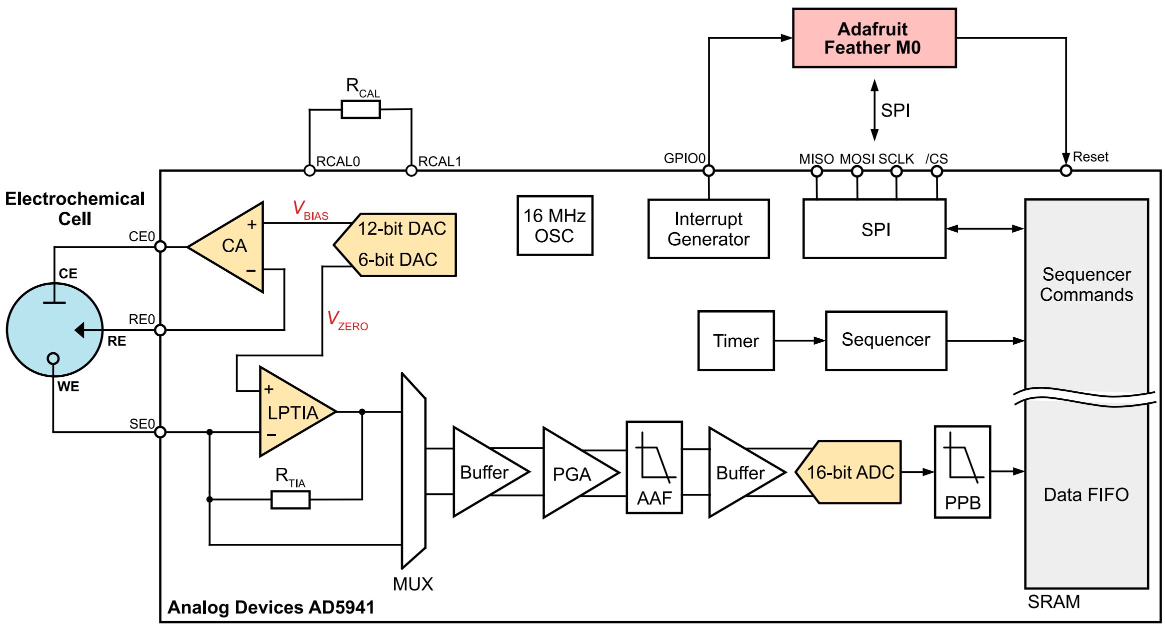

Figure 2. Block diagram of the FreiStat setup with the low-bandwidth loop, as configured for the measurements in this work.

and start sampling) and periodically triggered by a programmable internal wake-up timer.

Software Framework. The software framework comprises the following: (1) the firmware for the MCU communicating with the AD5941, (2) a Python library setting up the FreiStat hardware and receiving measured data from the MCU, and (3) further software providing a graphical user interface (GUI) or data storage/evaluation in the cloud. Different connections between the firmware and the Python library are possible using a serial connection with a USB cable connected to a computer running the Python library and, optionally, the GUI or using the User Datagram Protocol (UDP) with the FreiStat and the computer connected over Wi-Fi or other transmission routes. Also, the standalone operation of the FreiStat hardware with data storage on a SD card is possible. The Supporting Information (Figures S4 and S5) provides a more detailed treatment of the architecture of the software framework. To enable both open-source and commercial applications, we released the software framework under the MIT license. This work additionally demonstrates a typical IoT scenario using the IBM Cloud with the MQTT messaging protocol (Experimental Section). All code used in this work is available on GitHub (https://github.com/IMTEK-FreiStat).

Firmware Implementation of Voltammetry. A particularity of FreiStat compared to other embedded potentiostats is the use of the current averaging method for the linear scan or cyclic voltammetry measurements. In contrast to proper linear excitation (a linear ramp), embedded potentiostats and most of today's benchtop devices generate the applied potential ramp with a DAC producing a staircase instead. Accordingly, the resulting current signal is a sequence of step responses, leading to underestimating the true value when sampling at the end of each step. This effect may lead to wrong conclusions, especially for cyclic voltammetry to characterize noble metal electrodes, as is common in fuel cells, electrolysis, battery research, or neurotechnology. We demonstrated earlier that integrating the analog signal of the current response over each step in a staircase or taking the average of many digitized current readings spread along each step provides the same results quantitatively as with a true linear ramp.[25]

Figure 3 shows the implementation of this current averaging approach in the firmware. The scan rate and the step size

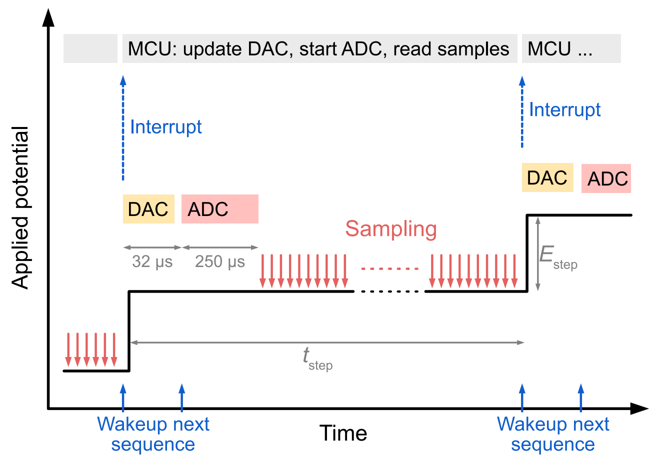

Figure 3. Timing diagram of the firmware implementation of voltammetry with a staircase approximating the linear potential ramp. A few hundred samples covering most of the step duration contribute to the mean value in each step, which is one current measurement value.

define the staircase. The minimal potential step at the 12-bit DAC is 537.24 μV. Typical values are a step size E_{step} of 2 mV for a scanrate of 100 mV/s. Accordingly, the step duration t_{step} is 20 ms.

Each step required setting the DAC, starting the ADC, and sampling the current. First, the DAC switches the potential, followed by communication with the MCU to update the sequencer. The MCU needs to calculate each DAC code at run time and send it to the AD5941 within one tick of the 32 kHz oscillator (below 32 μs). Next, the ADC starts and samples with a delay of 250 μs continuously until the end of the step. Depending on the oversampling rate, a few hundred readings

https://doi.org/10.1021/acs.analchem.3c02114
Anal. Chem. 2023, 95, 13003−13009

contribute to the mean value in each step. Apart from less than the first 300 μs, current readings over the whole step duration contribute to the mean value, forming one current measurement in the voltammetry experiment. This procedure is sufficient to approach a true integration (in the above example, with a step duration of 20 ms, the sampling would cover more than 98% of each step).

■ EXPERIMENTAL SECTION

Electrochemical and Biosensor Setup. The working electrodes were 3 mm disk platinum or glassy carbon electrodes (Gamry, U.S.A.) with a platinum rod as the counter electrode in the voltammetry measurements. The corrosion analysis used the PTC1 Paint Test Cell (Gamry, U.S.A) with a graphite rod as the counter electrode. The working electrode was a steel plate protected by Electroplating Tape 470 (3M, U.S.A.) with a circular 3 mm opening to limit the sample's area. Apart from the biosensor measurement with an on-chip Ag/AgCl electrode, the reference electrodes were Ag/AgCl glass electrodes filled with 3 M KCl.

The enzymatic lactate biosensor was a flexible strip-type microsensor.[26] A hydrogel membrane on the platinum working electrode (0.126 mm^2 area) contained the enzyme lactate oxidase. The electrode had no additional diffusion-limiting membrane to achieve a highly sensitive sensor.

For comparison, an Autolab PGSTAT128N (Metrohm, Germany) with the FI20 analog filter and integrator module, a CompactStat (Ivium Technologies, The Netherlands), and an EmStat Pico (PalmSens, The Netherlands) were used. The EmStat-Pico (firmware version 1.304) was connected using a UART-USB converter to a PC as recommended by the manufacturer and controlled with the PalmSens PSTrace software.

The cyclic voltammetry of platinum and the biosensor experiments used phosphate-buffered saline (PBS) pH 7.4, prepared from 85.18 mM Na_2HPO_4, 14.82 mM NaH_2PO_4, and 100 mM NaCl in deionized water, optionally with lactate by addition from 100 mM sodium L-lactate in PBS stock solution. Dissolved oxygen in the electrolyte for the platinum cyclic voltammograms was removed by bubbling with nitrogen for at least 10 min before and flushing above the liquid level during the experiments. One mM $K_4[Fe(CN)_6]$ in 100 mM KCl was the electrolyte for the voltammetry with a redox couple. 0.5 M NaCl in deionized water was used in the corrosion analysis.

All measurements were taken at room temperature (23 ± 2 °C).

Embedded Potentiostat. During all experiments, the FreiStat PCB hosting the AD5941 was stacked onto a Feather M0 Wifi board in addition to an Adalogger FeatherWing and a FeatherWing OLED with a 128 × 32 display (all from Adafruit Industries, USA). The Adalogger FeatherWing was equipped with a 2 GB micro SD card and CR1220 coin cell for the real-time clock (also when not used).

Cloud Application. We exploited the IBM Cloud as a cloud service for voltammetric measurements to demonstrate how the developed platform can be embedded into an IoT scenario. Deviating from the general approach of the FreiStat framework, this example required the MQTT protocol for data transfer to and from the cloud service. The Supporting Information (Figure S5) describes in more detail the architecture and services used in this work.

■ RESULTS AND DISCUSSION

Cyclic Voltammetry and Differential Pulse Voltammetry. The characterization experiments address two use cases of voltammetric measurements: current contribution from redox-active substances in the electrolyte, ideally at an inert working electrode, and from surface reactions of the electrode material itself. The latter is more challenging for embedded potentiostats. Therefore, we compared cyclic voltammograms of a platinum electrode recorded with FreiStat, benchtop devices, and EmStat Pico.

Figure 4A shows the results from the FreiStat in comparison to a benchtop device with an analog integrator (Autolab) and with a current averaging mode (Ivium). The potential step E_{step} of the applied staircase was 2 mV, resulting in an integration/averaging time of 40 ms, twice the period of the mains frequency (50 Hz). All three curves are the same within the repeatability of platinum cyclic voltammograms. Following the curve in the upward scan from around 0.2 V, the positive current is due to the oxidation of the platinum surface with water to PtO. Just at the upper turning point, the formation of molecular oxygen (O_2) sets in. On the reverse scan, the large negative current peak is from the reduction of the before-formed PtO. The features in the hydrogen adsorption/desorption region (marked by arrows) resolve clearly. Close

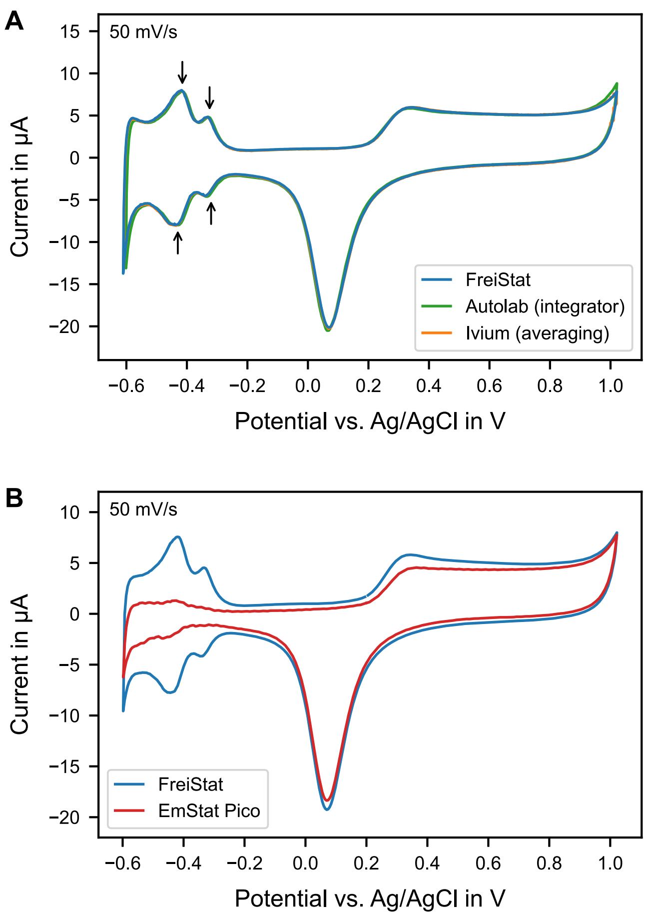

Figure 4. Cyclic voltammograms of a platinum electrode in nitrogen-flushed PBS comparing the FreiStat to benchtop devices (A) and the EmStat Pico module (B). The potential step E_{step} of the applied staircase was 2 mV in A and 5 mV in B.

to the lower turning potential, the downward tip is the formation of molecular hydrogen (H_2).[25]

In contrast, the EmStat Pico (Figure 4B) cyclic voltammogram deviates significantly. Depending on the chosen potential step, the result slightly varies, with the same overall appearance. The data shown is for an E_{step} of 5 mV, the value at which the EmStat Pico performed best. The charge within one cycle derived from the enclosed area is less than with the FreiStat. The most substantial deviation occurs in the hydrogen adsorption−desorption region, in which the involved reactions are very fast and accordingly complete already at the beginning of each step. The curve shape is typical when sampling the current only at the end or at a later fraction of the potential step. This finding supports our assumption that FreiStat's performance depends more on the firmware than the analog front end (comparable between the AD5941 and the EmStat Pico).

Figure 5A shows the results from cyclic voltammetry in a solution with a species forming a redox couple ($[Fe(CN)_6]^{3-}$/

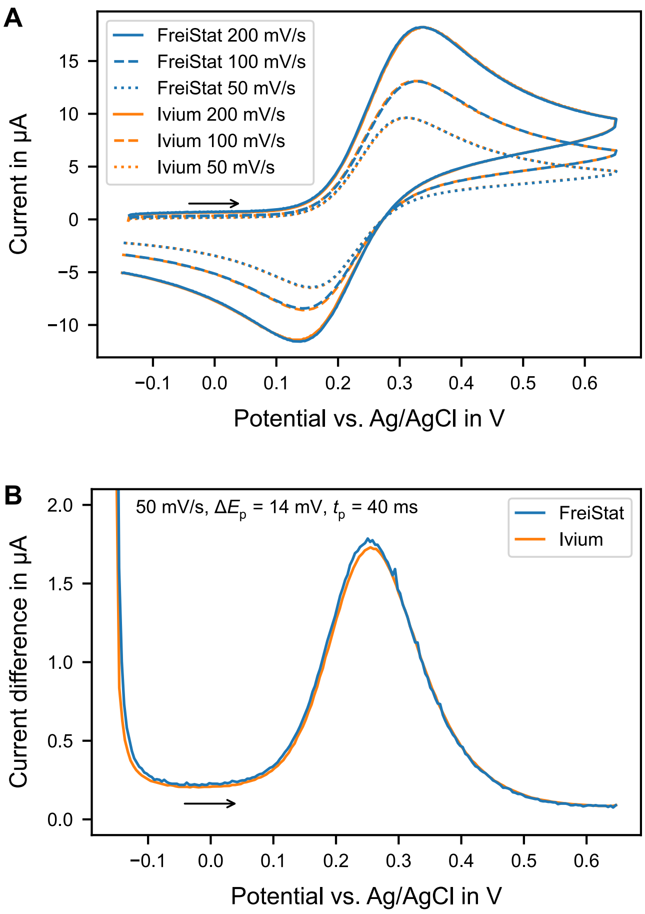

Figure 5. Cyclic voltammograms of a glassy carbon electrode with 1 mM $K_4[Fe(CN)_6]$ in 100 mM KCl (A) and a differential pulse voltammogram in the same electrolyte (B) comparing the FreiStat to a benchtop device.

$[Fe(CN)_6]^{4-}$). The resulting curves show the "Duck-shaped" characteristics, as predicted by theory. Initially, only the reduced form ($[Fe(CN)_6]^{4-}$) is in the solution, which is oxidized in the upward scan. After returning the potential, the before formed $[Fe(CN)_6]^{3-}$ gets reduced back with the cathodic peak less prominent and the electric current not reaching zero according to the theory considering the diffusion of the oxidized species away from the electrode. The magnitude and peak position change with the scanrate as expected. The FreiStat and the Ivium did not show any detectable difference. In Figure 5B the results from differential pulse voltammetry in the same electrolyte show no substantial difference either.

Chronoamperometry: Lactate Biosensors. Figure 6 shows the transient electric current signal with the response to

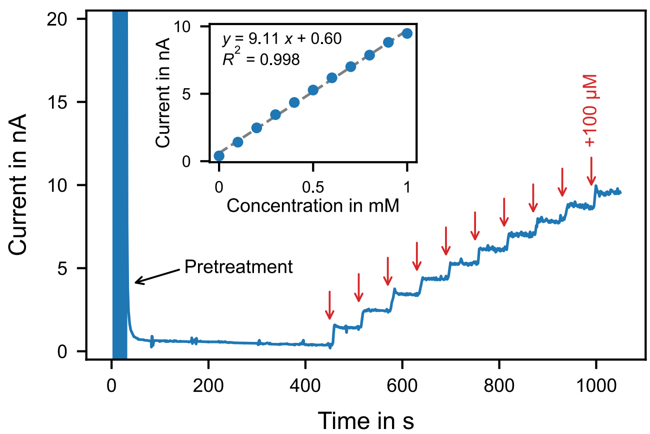

Figure 6. Chronoamperometric readout of a lactate biosensor in PBS. Time trace, each arrow represents the addition of 100 μM lactate, and calibration curve with fit in the linear range in the inset.

lactate addition to the stirred solution in 10 steps. The high resolution of the current measurement (54 pA for the used R_{TIA}) allows the pretreatment to be combined at levels of up to more than 1 μA with sensor signals in the nA-range and below. The covered concentration range matches well the relevant concentrations, e.g., for metabolic monitoring in organ-on-chip applications.[27] This value compares well to the human resting serum lactate levels of 0.5 to 2 mM. The measurement successfully demonstrated the applicability of FreiStat for biosensor measurements.

Corrosion Analysis in the Cloud. The corrosion analysis experiment aimed to demonstrate remote operation and data storage in the cloud. The cloud service enables calculations using Jupyter notebooks, e.g., for data evaluation, like the Tafel analysis, to estimate the corrosion rate. The corrosion cell with a steel sample connected to FreiStat was placed in a university lab while the operator controlled the experiment from a home office. Figure 7 shows the result of linear scan voltammetry with a scanrate of 1 mV s^{-1} in the range of ±200 mV relative to the open circuit potential (OCP) as a Tafel plot. The region at the lowest potential is the onset of hydrogen formation, followed by the area of oxygen reduction with its linear section, indicating mass transport limitation. Above the corrosion potential (zero crossing of the measured current), another linear region is metal corrosion. The Tafel slope equals 96.3 mV per decade, indicating the prevalence of two different reactions in the metal dissolution (theory predicts 118 mV for a one-electron process and 59 mV for a two-electron process at room temperature). The slope corresponds to an effective number of electrons of 1.2.

The experiment demonstrated the possibility of cloud-based corrosion monitoring. In a real application, such a system allows continuous monitoring by frequently checking a

https://doi.org/10.1021/acs.analchem.3c02114
Anal. Chem. 2023, 95, 13003−13009

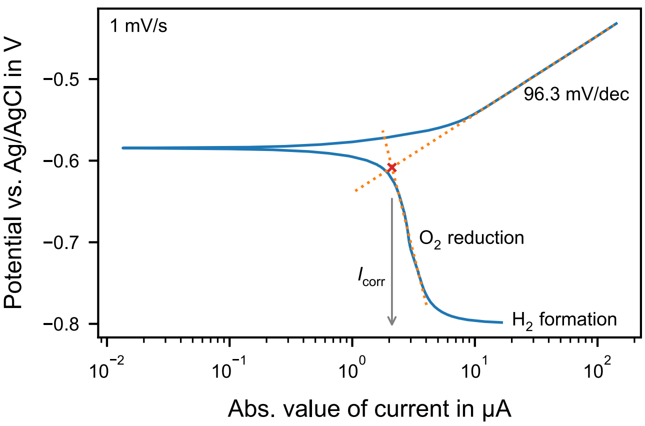

Figure 7. Corrosion analysis in the cloud: linear scan voltammetry of a steel sample in 0.5 M NaCl with air-saturated oxygenation. Evaluation of the measurement results by Tafel analysis predicts a corrosion rate of about 0.6 mm $year^{-1}$.

corrosion rate at remote places and indicating changes in the corrosion behavior as an early warning for future failure.

CONCLUSIONS

The developed FreiStat hardware prototype and software framework provide a powerful embedded potentiostat for performing various electrochemical measurements. By incorporating the AD5941 integrated circuit, the system suits applications with high constraints regarding size, power, and costs yet requires accurate measurements. These factors are crucial for IoT integration and monitoring in remote places. The emphasis on the proper firmware implementation of the electrochemical methods was justified, as demonstrated by various voltammetric measurements. The current averaging mode for cyclic voltammetry results in high-quality data comparable with benchtop devices and outperforms the state-of-the-art in embedded potentiostats. The biosensor measurements demonstrated the applicability of FreiStat in the lower nano-Ampere measurement range. Beyond the implemented electrochemical methods, the structure of the software framework allows the implementation of other measurement techniques or adaption for a specific cloud service, such as the IBM Cloud. For the first time, we demonstrated the realization of remote corrosion monitoring with an embedded potentiostat in the cloud. The developed open-source software framework facilitates the integration of electrochemical instrumentation into applications utilizing machine learning and other artificial intelligence.

ASSOCIATED CONTENT

Supporting Information

The Supporting Information is available free of charge at https://pubs.acs.org/doi/10.1021/acs.analchem.3c02114.

Circuit diagram and board layout of the FreiStat main board; cyclic voltammetry: fixed working electrode potential; software framework, including modes of operation; IoT example: IBM Cloud (PDF)

AUTHOR INFORMATION

Corresponding Author

Jochen Kieninger − *Laboratory for Electrical Instrumentation and Embedded Systems, IMTEK − Department of Microsystems Engineering, Laboratory for Sensors, IMTEK − Department of Microsystems Engineering, and BrainLinks−BrainTools Center, University of Freiburg, 79110 Freiburg, Germany;* orcid.org/0000-0001-8220-8814; Email: kieninger@imtek.uni-freiburg.de

Authors

David Bill − *Laboratory for Sensors, IMTEK − Department of Microsystems Engineering, University of Freiburg, 79110 Freiburg, Germany*

Mark Jasper − *Laboratory for Sensors, IMTEK − Department of Microsystems Engineering, University of Freiburg, 79110 Freiburg, Germany*

Andreas Weltin − *Laboratory for Electrical Instrumentation and Embedded Systems, IMTEK − Department of Microsystems Engineering, Laboratory for Sensors, IMTEK − Department of Microsystems Engineering, and BrainLinks−BrainTools Center, University of Freiburg, 79110 Freiburg, Germany;* orcid.org/0000-0001-8288-8266

Gerald A. Urban − *Laboratory for Sensors, IMTEK − Department of Microsystems Engineering and BrainLinks−BrainTools Center, University of Freiburg, 79110 Freiburg, Germany*

Stefan J. Rupitsch − *Laboratory for Electrical Instrumentation and Embedded Systems, IMTEK − Department of Microsystems Engineering and BrainLinks−BrainTools Center, University of Freiburg, 79110 Freiburg, Germany*

Complete contact information is available at: https://pubs.acs.org/10.1021/acs.analchem.3c02114

Author Contributions

[#]D.B. and M.J. contributed equally to this paper.

Notes

The authors declare no competing financial interest.

ACKNOWLEDGMENTS

Partial funding from the Federal Ministry for Economic Affairs and Climate Action, Germany, Project “Cooperative Development of a Comprehensive Integrated Autonomous Underwater Monitoring Solution (CIAM)”, No. 03SX540J, and within the BrainLinks-BrainTools Center, Project “INTEREST” is gratefully acknowledged.

REFERENCES

(1) Mayer, M.; Baeumner, A. J. *Chem. Rev.* **2019**, *119* (13), 7996−8027.
(2) Prabhu, G. R. D.; Urban, P. L. *Chem. Rev.* **2020**, *120* (17), 9482−9553.
(3) Rowe, A. A.; Bonham, A. J.; White, R. J.; Zimmer, M. P.; Yadgar, R. J.; Hobza, T. M.; Honea, J. W.; Ben-Yaacov, I.; Plaxco, K. W. *PLoS One* **2011**, *6* (9), e23783.
(4) Steinberg, M. D.; Kassal, P.; Kereković, I.; Steinberg, I. M. *Talanta* **2015**, *143*, 178−183.
(5) Dryden, M. D. M.; Wheeler, A. R. *PLoS One* **2015**, *10* (10), e0140349.
(6) Giordano, G. F.; Vicentini, M. B. R.; Murer, R. C.; Augusto, F.; Ferrão, M. F.; Helfer, G. A.; da Costa, A. B.; Gobbi, A. L.; Hantao, L. W.; Lima, R. S. *Electrochim. Acta* **2016**, *219*, 170−177.
(7) Dobbelaere, T.; Vereecken, P. M.; Detavernier, C. *Hardwarex* **2017**, *2*, 34−49.
(8) Ainla, A.; Mousavi, M. P. S.; Tsaloglou, M.-N.; Redston, J.; Bell, J. G.; Fernández-Abedul, M. T.; Whitesides, G. M. *Anal. Chem.* **2018**, *90* (10), 6240−6246.

(9) Mercer, C.; Bennett, R.; Conghaile, P. Ó.; Rusling, J. F.; Leech, D. *Sensors Actuators B Chem.* **2019**, *290*, 616−624.
(10) Bianchi, V.; Boni, A.; Fortunati, S.; Giannetto, M.; Careri, M.; De Munari, I. *IEEE T Instrum Meas* **2020**, *69* (6), 3232−3240.
(11) Jenkins, D. M.; Lee, B. E.; Jun, S.; Reyes-De-Corcuera, J.; McLamore, E. S. *J. Electrochem. Soc.* **2019**, *166* (9), B3056−B3065.
(12) Irving, P.; Cecil, R.; Yates, M. Z. *Hardwarex* **2021**, *9*, e00163.
(13) Ahmad, R.; Surya, S. G.; Sales, J. B.; Mkaouar, H.; Catunda, S. Y. C.; Belfort, D. R.; Lei, Y.; Wang, Z. L.; Baeumner, A.; Wolfbeis, O. S.; Alshareef, H. N.; Salama, K. N. *2019 IEEE Sensors* **2019**, *00*, 1−4.
(14) Escobedo, P.; Erenas, M. M.; Martínez-Olmos, A.; Carvajal, M. A.; Gonzalez-Chocano, S.; Capitán-Vallvey, L. F.; Palma, A. J. *Biosens Bioelectron* **2019**, *141*, 111360.
(15) Hoilett, O. S.; Walker, J. F.; Balash, B. M.; Jaras, N. J.; Boppana, S.; Linnes, J. C. *Sensors* **2020**, *20* (8), 2407.
(16) Pozo, B.; Gorostiza, E. F. de; Eletxigerra, U.; Mabe, J.; Martínez, A. *Active Passiv Smart Struct Integr Syst. IX* **2020**, *11376*, 113760Q−113760Q.
(17) Corva, D. M.; Adams, S. D.; Doeven, E. H.; Hashemi, P.; Kouzani, A. Z. *2022 29th IEEE Int. Conf Electron Circuits Syst. Icecs* **2022**, *00*, 1−4.
(18) Szobolovszky, R.; Donovalova, J. *2022 14th Int. Conf Adv. Semicond Devices Microsystems Asdam* **2022**, *00*, 1−4.
(19) Han, J.; Stine, J. M.; Chapin, A. A.; Ghodssi, R. *Anal Methods-uk* **2023**, *15* (9), 1096−1104.
(20) *EmStat Pico Datasheet*, Rev. 10-2021-007; PalmSens BV, The Netherlands, 2021.
(21) Lopin, P.; Lopin, K. V. *PLoS One* **2018**, *13* (7), e0201353.
(22) Adams, S. D.; Doeven, E. H.; Tye, S. J.; Bennet, K. E.; Berk, M.; Kouzani, A. Z. *Ieee T Neur Sys Reh* **2020**, *28* (1), 133−142.
(23) Krorakai, K.; Klangphukhiew, S.; Kulchat, S.; Patramanon, R. *Appl. Sci.* **2021**, *11* (1), 392.
(24) Kieninger, J. *Electrochemical Methods for the Micro- and Nanoscale, Theoretical Essentials, Instrumentation and Methods for Applications in MEMS and Nanotechnology*; De Gruyter: Berlin/Boston, 2022. DOI: 10.1515/9783110649758.
(25) Weltin, A.; Kieninger, J. *J. Neural Eng.* **2021**, *18* (5), 052001.
(26) Weltin, A.; Kieninger, J.; Enderle, B.; Gellner, A.-K.; Fritsch, B.; Urban, G. A. *Biosens Bioelectron* **2014**, *61*, 192−199.
(27) Dornhof, J.; Kieninger, J.; Muralidharan, H.; Maurer, J.; Urban, G. A.; Weltin, A. *Lab Chip* **2022**, *22* (2), 225−239.

https://doi.org/10.1021/acs.analchem.3c02114
Anal. Chem. 2023, 95, 13003−13009